Available online at www.sciencedirect.com
SCIENCE DIRECT®
Journal of Photochemistry and Photobiology A: Chemistry 158 (2003) 83–100
Journal of Photochemistry and Photobiology A:Chemistry
www.elsevier.com/locate/jphotochem

Competitive electron transfers in model ionic triad systems: MD simulations

Maria Hilczer [a,b], M. Tachiya [a,*]

[a] National Institute of Advanced Industrial Science and Technology, Tsukuba Central 5, 1-1-1 Higashi, Ibaraki 305-8565, Japan
[b] Institute of Applied Radiation Chemistry, Technical University, Wroblewskiego 15, 93-590 Lodz, Poland

Received 25 March 2002; accepted 1 July 2002

Abstract

We present the second part of the work [J. Phys. Chem. 100 (1996) 8815] devoted to electron transfer (ET) reactions in model triad systems. A model supramolecule is the ionic triad D^+–$A1^-$–A2 immersed in acetonitrile solvent at room temperature. The ET rate constants for both the charge separation (the forward ET) and the charge recombination (the backward ET) are expressed in terms of the two-dimensional (2D) statistical distribution of the respective solvent polarization coordinates. This distribution for the triad with various angular arrangements of the subunits has been evaluated by the MD computer simulation for the molecular model of the solvent. The dependence of the yield of the charge-separated state D^+–A1–$A2^-$ on the triad geometry and the free energy changes of the forward and the backward ETs as well as the conditions that maximize the yield of the forward ET have been considered.

Keywords: Computer simulation; Molecular dynamics; Photoinduced electron transfer; Triad system

1. Introduction

Electron transfer (ET) in supramolecular systems is a subject of intensive experimental [1–28] and theoretical [29–54] research, which have an important practical implication. It has been proven possible to prepare synthetic molecular devices that can be used for capturing and storing solar energy. Their efficiency is, however, still beneath the level of the most famous natural electronic devices such as the reaction centers (RCs) of photosynthetic organisms.

Theoretical approach to ETs in multicenter systems immersed in protein or polar solvents requires definition of an appropriate number of intramolecular and solvent-dependent reaction coordinates. The former coordinates are connected with the internal reorganization of a supramolecule during particular charge transfer processes, whereas the latter describe the effect of fluctuation of the surrounding medium. For rigid supramolecular systems in solvents of high polarity the set of reaction coordinates can be limited to the solvent polarization coordinates. It has been shown that the competitive or sequential ETs in a rigid triad system can be modeled using two polarization coordinates and, consequently, the two-dimensional (2D) free energy surfaces of the reactant and the product states [29–32].

Pairs of orthogonal reaction coordinates were introduced by Marchi et al. [34] and Parson et al. [35] in their computer simulations of the competitive charge separation reactions in the bacterial photosynthetic RC. Results of the former group supported the direct ET (superexchange) from unit 1 of the triad (special pair composed of a bacteriochlorophyll dimer) to unit 3 (bacteriopheophytin). Results of the latter group predicted the possibility of the sequential ETs: from 1 to 2 (bacteriochlorophyll) and then from 2 to 3. Warshel et al. [37] suggested that divergence of the simulation results arose from incomplete treatment of dielectric effects in the Marchi's calculations. All these groups of workers used, however, one-dimensional (1D) free energy curves, instead of 2D free energy surfaces, to analyze their simulation data. Fushiki and Tachiya [38] have constructed the correct 2D free energy functions for the two primary ETs in the bacterial RC from the results of the aforementioned simulations. Their conclusions supported the two-step mechanism of charge separation in the RC. The authors underlined that if the rate of fluctuation of solvent surrounding the triad is slow compared with rates of the two competitive ETs, then these ETs interfere with each other and this makes it impossible to describe them separately based on 1D free energy curves. Contrary, in the nonadiabatic limit the equilibrium

* Corresponding author.
E-mail addresses: hilczerm@mitr.p.lodz.pl (M. Hilczer), m.tachiya@aist.go.jp (M. Tachiya).

1010-6030/03/$ – see front matter
doi:10.1016/S1010-6030(03)00021-2

distribution in the free energy surface of the initial state of the triad is maintained during ETs and both reactions occur independently [29–32,38]. Thus, each of them can be analyzed using a pair of appropriate 1D free energy curves: one curve for the initial state and one for the final state. The initial state curves $G_{is}(q_1)$ and $G_{is}(q_2)$ for the two competitive ETs are, however, different even in the nonadiabatic limit.

Recently, Zusman and Beratan [39] developed the theory of ET in three-center systems immersed in a dielectric-continuum solvent. They described ET as arising from 2D diffusion over two statistically independent reaction coordinates, which were defined similarly as in [34]. Their theory describes competition between sequential and superexchange ET mechanisms, and includes the solvent dynamics control of the overall reaction rate. The dynamical solvent effect in the dielectric-continuum limit was also considered in a theory developed by Okada et al. [40], which concerns ETs among many electronic states coupled to multidimensional diffusive nuclear modes. The theory has been applied to description of the *nonequilibrium sequential* ETs in a supramolecular triad system composed of donor–medium–acceptor (DMA) molecules. In other words, they considered ET from D*MA to D^+M^-A, followed by another ET from D^+M^-A to D^+MA^- without thermal equilibration of the state D^+M^-A. They found a nonmonotonic dependence of the overall donor-to-acceptor ET rate constant k on the solvation time scale τ_s. The function $k(\tau_s)$ appeared to increase in the region of small τ_s and decrease in the slow solvation limit. Najbar and co-workers [41] applied the theory of the nonadiabatic ET reactions based on the stochastic Liouville equation to model DAA triad systems in a continuum dielectric solvent. Fushiki and Tachiya [30] expressed the two-step ETs in a model linear triad DAA surrounded by polar, structureless solvent in terms of the dynamics of a Brownian particle on the 2D free energy surface $F_I(q_1, q_2)$ of the intermediate state D^+A^-A.

In the majority of papers concerning ETs in three-center systems, a polar solvent was treated as a *dielectric continuum* characterized by specific values of the static and optical dielectric constants. Our previous paper [32] introduced a *molecular model* of solvent (acetonitrile) and showed how it affects description of the competitive ET reactions in a model rigid supramolecule with various spatial arrangements of the subunits. One of the triad considered there was the D–A1–A2 system that produces after photoexcitation the ionic states D^+–$A1^-$–A2 or D^+–A1–$A2^-$.

The present work is a logical continuation and completion of those studies. It is devoted to ETs which occur in the model, *ionic* triads D^+–$A1^-$–A2 immersed in acetonitrile solvent at room temperature. One of these ETs is the backward reaction, which leads to reformation of the neutral system D–A1–A2, the other is the forward ET resulting in the charge-separated state D^+–A1–$A2^-$. The reaction coordinates for these two processes are defined as $q_1 = e(V_2 - V_1)$ and $q_2 = e(V_2 - V_3)$, where V_1, V_2 and V_3 stand for the electrostatic potential at D^+, $A1^-$ and A2, respectively. We apply the MD computer simulation method to calculate the statistical distribution $\varphi(q_1, q_2)$ and, consequently, the free energy surface of the D^+–$A1^-$–A2 state. We consider the nonadiabatic limit (fast solvation) at which both reactions can run parallel on this energy surface. The reaction coordinates are random variables. We describe static and dynamical stochastic properties of the reaction coordinates and discuss the influence of the solvent, the triad geometry, and the free energy changes on the two processes on the basis of these properties. We also consider the competition between the forward and the backward ET reactions and the conditions that maximize the yield of the former process. Our triad is not supposed to mimic any specific experimental system. Our intention is to show the role of the solvent, for which we employ a realistic *molecular* model [55] that has been proven to reproduce some structural and dielectric properties of the bulk phase [56,57]. We compare some results for the ionic system with those for the neutral triad and discuss some conclusions drawn from the present model in relation to the available experimental data.

The remainder of the paper is organized as follows: In Section 2 we describe details of the performed computer simulations. In Section 3.1 we present the 2D and marginal (1D) probability distribution functions and their dependence on the angular arrangement of the triad subunits. The dynamical properties of the reaction coordinates are discussed based on the time auto- and cross-correlation functions in Section 3.2. We compare here the dynamics of solvation of the particular subunits of the triad with that of the separately solvated molecules or ions. In Section 3.3 we present the rate constants for the forward and backward ETs and discuss the efficiency of the former process. Finally, in Section 3.4, we describe the solvent structure and the charge distribution around the ionic triads and compare them with respective data for the neutral triad systems.

2. Outline of calculation

Chromophores of the D^+–$A1^-$–A2 system were modeled by two simple ions (labeled 1 and 2) and one atom (labeled 3), and surrounded by 497 acetonitrile molecules. The triad was immobile during simulation runs and a constant value of $r = 5.5$ Å was assumed as the distance between the central and each of the side subunits. We considered several different angular arrangements of the triad, which were characterized by the angle β between axes connecting $A1^-$ with D^+ and A2, respectively. The values of β assumed for particular runs were 60, 90, 120, and 180°.

CH_3CN–CH_3CN interactions were described by the six-site potential developed by Böhm et al. [55]. In this potential the sites are located on the respective atoms of an acetonitrile molecule and each site of one molecule interacts with every site on another molecule through the standard 6–12 Lennard–Jones and the Coulomb potentials. The acetonitrile molecule is treated as a rigid object, with

bond lengths which are deduced from diffraction data on the liquid and equal to: $r_{C_1–H} = 1.087$ Å, $r_{C_1–C_2} = 1.460$ Å, $r_{C_2–N} = 1.170$ Å, $r_{H–H} = 1.771$ Å and the bond angle $\angle(H–C_1–C_2) = 109.8^\circ$. In the above notation C_1 and C_2 stand for the carbon atoms in the methyl and cyanide groups, respectively. This model potential is widely used in MD simulations and gives a good description of the structural, dynamical and dielectric properties of both the bulk liquid [56,57] and the acetonitrile clusters [58]. The interactions of the triad subunits with the sites on a solvent molecule were described by the 6–12 Lennard–Jones plus Coulomb potentials. A value of $\varepsilon = 18k_B$ was taken as the Lennard–Jones well depth and $s = 4.9$ Å as the collision diameter for each of the solutes. The solute–solvent interactions as well as interactions between unlike atoms in different acetonitrile molecules were approximated using the Lorentz–Berthelot mixing rules [59].

The MD program used for the calculations is based on the MDMPOL coded by Smith and Fincham [60], and calculates the time evolution of the system in the NVE ensemble using a leapfrog algorithm for the center-of-mass motions and a leapfrog-quaternion algorithm for the angular motions of the solvent molecules [59]. Our system of 500 particles was confined to the cubic box of side length of 35.1214 Å, and we employed the usual periodic boundary conditions as well as the Ewald summation of the electrostatic interactions. The average temperatures in all equilibrium runs were 291 ± 4.9 K. Equations of motion of solvent molecules were integrated with the time step of 2 fs, which ensured that the total energy of the system was conserved within less than 0.09% over the course of a 60 ps equilibrium trajectory. Simulation runs of about 700 ps, performed for each angular arrangement of the triad, were divided into 12 separate runs between which we annealed the system, i.e., the system was first warmed up to a temperature of about 600 K and then gradually cooled back to 291 K. This procedure allowed us to avoid trapping of the solvent molecules into some artificial configurations in the vicinity of the solute atoms.

The electrostatic potential energies eV_1, eV_2 and eV_3, produced by solvent molecules at the centers of D^+, $A1^-$ and A2, respectively, were calculated after every three time steps of the equilibrium trajectory of the system and were recorded sequentially during the production period of the simulation. Long-range electrostatic interactions were included into the potential experienced by each subunit of the triad by applying an anisotropic approximation to the Ewald summation [61]. In this approximation the Ewald potential for a pair of point charges is given by the formula

$$E(r) = \frac{1}{r} + a_1 r^2 + a_2 r^4 + a_3 r^6 + a_4 r^8 + a_5 T_4 + a_6 T_6 + a_7 T_8 + a_8 T_4 r^2 + a_9 T_6 r^2 + a_{10} T_4 r^4 \quad (1)$$

where $T_n = x^n + y^n + z^n$, and $r = (x^2 + y^2 + z^2)^{1/2}$ denotes the distance between the test charge at each subunit of the triad and a partial charge on a particular atom of an acetonitrile molecule. Distances in Eq. (1) are expressed in units of side length of the simulation box and the constants a_1 to a_{10} have the following values: 2.094395, −4.506792, 6.651269, −10.86613, 7.511320, 17.07159, 60.53989, −23.27944, −113.0078, and 65.19680, respectively. Summation of the terms in Eq. (1), performed for all the partial charges of all the acetonitrile molecules in the simulation box, gives the electrical potential at each subunit of the triad. Formula (1) is relatively simple and allows us to obtain more precise values for the interaction energy than the spherical approximations to the Ewald sum.

The potential energy differences $e\Delta V_{21} = e(V_2 - V_1)$ between the $A1^-$ and D^+ subunits and $e\Delta V_{23} = e(V_2 - V_3)$ between the $A1^-$ and A2 subunits are the random variables, which we denote as q_1 and q_2, respectively. These random variables are the appropriate reaction coordinates for description of the competitive backward and forward ET reactions in the ionic triad system [29,30,62].

The joint probability distribution function $\varphi(q_1, q_2)$ of the variables q_1 and q_2 and the marginal probability distributions $\varphi_i(q_i)$ of particular q_i's for all considered angular arrangements of the triad were constructed as histograms of the data collected during the equilibrium (production) period of the simulations. The performed simulation runs allowed us to obtain relatively smooth 1D and 2D probability distribution functions. They were also sufficient for calculation of the time auto-correlation and cross-correlation functions (see Section 3.2), which characterize the classical dynamics of the considered random variables. The calculations were performed on the IBM RISC System/6000 Power Cluster which executes 134 Mflops in a one-processor computation.

3. Results and discussion

3.1. Static stochastic properties of the reaction coordinates

For the D^+–$A1^-$–A2 state, that we refer to as redox State I, the back ET can lead to the ground state D–A1–A2 (State 0) and the forward ET to the charge-separated state D^+–A1–$A2^-$ (State II). The differences between energies of the States I and 0 or I and II correspond, respectively, to the energy gaps for the backward or forward transfers. Assuming that the electron interacts with its environment only electrostatically, each of these energy gaps can be expressed by the difference in the electrostatic energy of the transferred electron before and after transfer, i.e., by $q_1 = e\Delta V_{21} = e(V_2 - V_1)$ for the backward and $q_2 = e\Delta V_{23} = e(V_2 - V_3)$ for the forward ETs. The electrostatic potentials V_2, V_1 and V_3 are generated by the solvent at the positions of the actual electron donor $A1^-$ (unit 2) and the acceptor D^+ (unit 1) and A2 (atom 3), respectively.

We apply q_1 and q_2 as the reaction coordinates for the competitive ET processes in our ionic triad and connect the rates of these ETs with the joint probability distribution

function $\varphi(q_1, q_2)$ constructed for the solvated D^+–$A1^-$–A2 system. Within the framework of the linear response approximation $\varphi(q_1, q_2)$ is a 2D Gaussian

$$\varphi(q_1, q_2) = \frac{1}{2\pi\sigma_1\sigma_2\sqrt{1-\rho^2}} \exp\left\{-\frac{1}{2(1-\rho^2)}\left[\left(\frac{q_1-m_1}{\sigma_1}\right)^2 - 2\rho\frac{q_1-m_1}{\sigma_1}\frac{q_2-m_2}{\sigma_2} + \left(\frac{q_2-m_2}{\sigma_2}\right)^2\right]\right\} \quad (2)$$

where $m_1 = \langle e\Delta V_{21}\rangle_I$ and $m_2 = \langle e\Delta V_{23}\rangle_I$ are the ensemble averages

$$\sigma_1^2 = \langle \delta q_1^2\rangle_I = \langle (e\Delta V_{21} - m_1)^2\rangle_I,$$
$$\sigma_2^2 = \langle \delta q_2^2\rangle_I = \langle (e\Delta V_{23} - m_2)^2\rangle_I \quad (3)$$

are the fluctuations or variances of the respective potential energy differences calculated for the redox State I, and

$$\rho = \frac{\langle \delta q_1 \delta q_2\rangle_I}{\sigma_1\sigma_2} \quad (4)$$

is the correlation coefficient expressed by the covariance $\sigma_{12}^2 = \langle \delta q_1 \delta q_2\rangle_I$ of the random variables q_1 and q_2.

Linear response theory predicts also that the probability distribution function $\varphi_i(q_i)$ of each reaction coordinate q_i ($i = 1, 2$) is a 1D Gaussian. Parameters m_i, ${\sigma_i}^2$, and ρ of the 1D and 2D Gaussians depend on the angular arrangement of the triad subunits and we calculate them directly from the results of MD simulations. The obtained values of m_i and ${\sigma_i}^2$ together with their statistical errors are listed in Table 1. To estimate the errors we use a standard procedure described in [59]. The error of a mean m_i is expressed by σ_i divided by the square root of the number of *uncorrelated* solvent structures, i.e., as $\sigma_i\sqrt{f_{si}/n_{run}}$, where n_{run} stands for a total number of structures collected during the simulation and f_{si} is a statistical inefficiency factor estimated from a respective time auto-correlation function (cf. Fig. 5). This factor was dependent on the triad geometry and its values for all considered means were within an interval from 50 to 80 (f_{si}'s obtained for m_1 were higher than those for m_2). The errors in variances are determined by employing Eq. (6.23) of [59]. Figs. 1 and 2 present the distributions $\varphi_i(q_i)$ for the reaction coordinates q_i associated with the backward and forward ETs, respectively. Dotted lines in the figures show $\varphi_i(q_i)$ calculated as histograms from the respective MD data, whereas full lines are the Gaussian approximations to these histograms. The latter are calculated by the nonlinear regression method based on the Levenberg–Marquardt minimization algorithm. For all fittings performed the chi-square values do not exceed $2.8 \times 10^{-4}\,eV^{-2}$ and the standard errors obtained for Gaussian parameters m and σ are of the order of 0.001 eV. The optimized values of m_i and σ_i^2 agree, within the estimated errors, with the corresponding MD values given in Table 1.

The spatial arrangement of the D^+–$A1^-$–A2 system has rather small influence on $\varphi_1(q_1)$. The position of $\varphi_2(q_2)$ depends, however, considerably on the triad *shape*. To explain these relations we compare the parameters of the Gaussian distributions for the reaction coordinates $q_1 = e\Delta V_{21}$ and $q_2 = e\Delta V_{23}$ with those for the electrical potential eV_i ($i = 1, 2, 3$) produced by the solvent separately on each component of the triad. The respective data are included in Table 1. The average potential at the center of D^+ and $A1^-$ does not depend considerably on the triad geometry. On the contrary, the value of $\langle eV_3\rangle$ depends strongly on the triad shape and this dependence results mainly in the aforementioned shift of the distribution function of the reaction coordinate q_2. The positive electrostatic potential at the center of the uncharged moiety A2 shows an asymmetry

Table 1
Parameters of Gaussian distributions of the reaction coordinates $q_1 = e\Delta V_{21}$ and $q_2 = e\Delta V_{23}$, and the potentials eV_i, which are generated by the solvent on particular triad subunits[a]

	$\beta = 60°$	$\beta = 90°$	$\beta = 120°$	$\beta = 180°$
Backward ET, q_1				
m_1	4.792 ± 0.009	4.841 ± 0.009	4.849 ± 0.008	4.881 ± 0.009
σ_1^2	0.128 ± 0.003	0.128 ± 0.003	0.129 ± 0.003	0.136 ± 0.003
Forward ET, q_2				
m_2	2.052 ± 0.008	1.308 ± 0.007	1.021 ± 0.007	0.854 ± 0.008
σ_2^2	0.116 ± 0.003	0.111 ± 0.002	0.110 ± 0.002	0.120 ± 0.003
D^+ subunit				
$\langle eV_1\rangle$	−2.556 ± 0.008	−2.615 ± 0.008	−2.616 ± 0.007	−2.630 ± 0.007
$\langle \delta(eV_1)^2\rangle$	0.122 ± 0.002	0.117 ± 0.002	0.119 ± 0.002	0.120 ± 0.002
$A1^-$ subunit				
$\langle eV_2\rangle$	2.236 ± 0.007	2.226 ± 0.007	2.233 ± 0.007	2.250 ± 0.007
$\langle \delta(eV_2)^2\rangle$	0.090 ± 0.002	0.090 ± 0.002	0.088 ± 0.002	0.094 ± 0.002
A2 subunit				
$\langle eV_3\rangle$	0.184 ± 0.007	0.918 ± 0.007	1.212 ± 0.007	1.396 ± 0.007
$\langle \delta(eV_3)^2\rangle$	0.105 ± 0.002	0.103 ± 0.002	0.106 ± 0.002	0.103 ± 0.002

[a] The mean values are in eV and variances in eV^2.

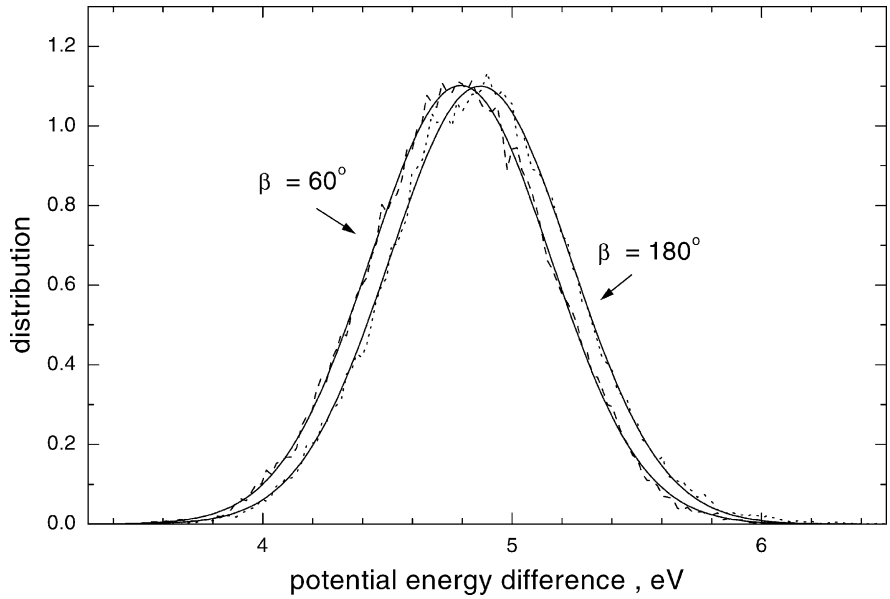

Fig. 1. Distributions of the reaction coordinate $q_1 = e\Delta V_{21}$ connected with the back ET for the regular triangle ($\beta = 60°$) and linear ($\beta = 180°$) system D^+–$A1^-$–A2 in acetonitrile at $T = 291$ K. β is the angle between directions of the D^+–$A1^-$ and $A1^-$–A2 bonds. Results of the MD simulation (dashed line) are fitted by the Gaussian function (full line).

in solvation of the triad system. This asymmetry is also seen in the solvation energies of the charged species. Multiplying the average potential at a given subunit by a charge located on the subunit, we obtain the electrostatic solvent–solute interaction energy E_{el}. Yu and Karplus [63] showed that this quantity can approximate quite reasonably the electrostatic free energy of solvation F_{el} via the relation $F_{el} \cong 0.5E_{el}$. The energy F_{el} calculated for the cation subunit of the triad appears to be more negative than that for the $A1^-$. A similar result was found for free, simple ions solvated in acetonitrile [64] and also for the molecular ions *N*,*N*-dimethylaniline$^+$ and anthracene$^-$ in the same solvent [65].

The width of the electrostatic potential difference distribution $\varphi_i(q_i)$ is related to the solvent reorganization energy λ_i, via

$$\sigma_i^2(\beta) = 2k_B T\lambda_i(\beta) \tag{5}$$

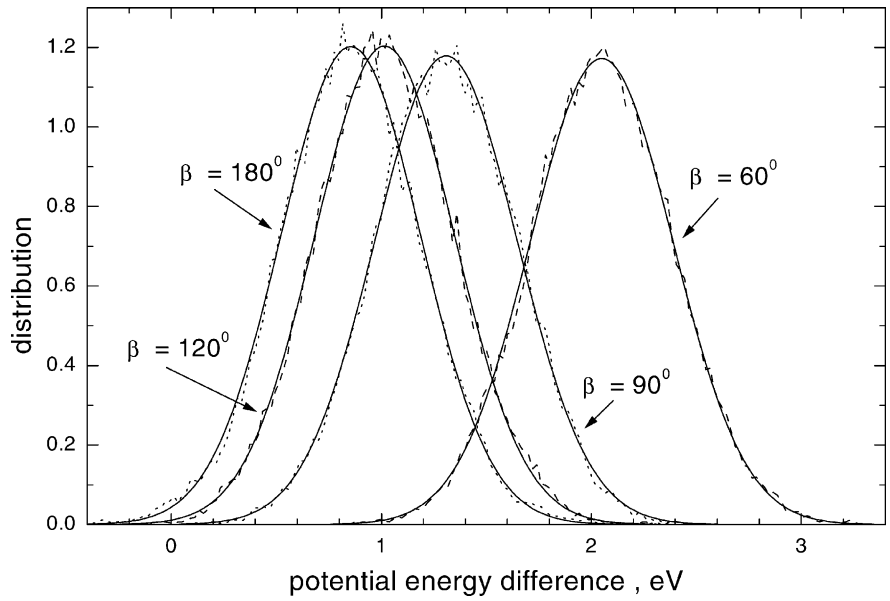

Fig. 2. Distributions of the reaction coordinate $q_2 = e\Delta V_{23}$ connected with the forward ET for different arrangements of the D^+–$A1^-$–A2 triad. Results of the MD simulations (dashed lines) are fitted by the Gaussian functions (full lines). Acetonitrile solution, $T = 291$ K.

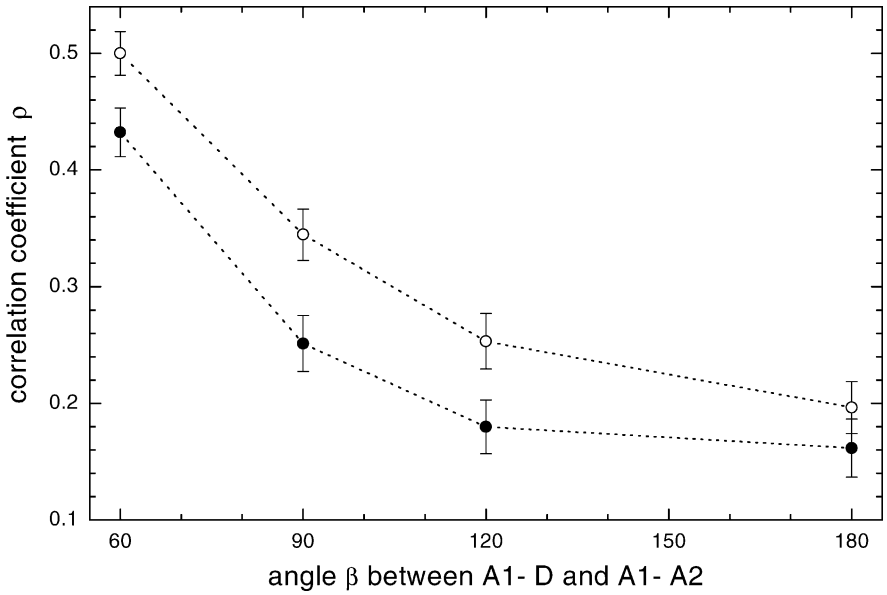

Fig. 3. Correlation coefficient ρ between reaction coordinates q_1 and q_2 as a function of the angle β calculated for the D^+–$A1^-$–A2 triad (black circles with error bars) and for the corresponding neutral system D–A1–A2 (open circles with error bars).

The reorganization energies associated with the backward and forward ETs are, on the average, 2.60 ± 0.06 and 2.28 ± 0.05 eV, respectively, and their dependence on the spatial arrangement of the triad is rather weak.

Fig. 3 presents the coefficient of correlation ρ between reaction coordinates q_1 and q_2 as a function of β. The values of $\rho(\beta)$ for the ionic triad are shown as black circles, whereas open circles show the correlation coefficients obtained for the corresponding neutral system D–A1–A2 [32]. Errors in the MD values of $\rho(\beta)$, which are presented in the figure, were calculated for ionic and neutral triads as $[1 - \rho^2(\beta)]/\sqrt{f_{si}/n_{run}}$. The correlation between reaction coordinates for the ionic triad is considerably weaker compared with that for the neutral triad. In the latter system motions of solvent molecules are constrained mostly by the hindered rotation effects. In the former system, however, we have additionally strong electrostatic interactions between the ionic components of the triad and the partial charges distributed on the acetonitrile molecules. Clearly, these interactions reduce correlation between quantities that depend on fluctuations in molecular arrangement in the vicinity of the triad.

3.2. Dynamical stochastic properties of the reaction coordinates

To characterize the dynamical behavior of the solvent and its relation to that of the reaction coordinates, we employ two kinds of equilibrium time auto-correlation functions (tacfs) defined by the relations

$$C_{V_i}(t) = \frac{\langle \delta V_i(0) \delta V_i(t) \rangle_I}{\sigma^2_{V_i}}, \quad i = 1, 2, 3 \tag{6}$$

with i running over the triad subunits D^+, $A1^-$, and A2, respectively, and

$$C_i(t) = \frac{\langle \delta q_i(0) \delta q_i(t) \rangle_I}{\sigma_i^2}, \quad i = 1, 2 \tag{7}$$

for the reaction coordinates q_1 and q_2. $\delta V_i(t)$ stands for the instantaneous fluctuation of the electrical potential $V_i(t)$ at the center of ith moiety of the triad from its equilibrium average value and $\delta q_i(t)$ is the fluctuation of the coordinate $q_i(t)$. The error of a time correlation function $C(t)$ is generally expressed as $(2t'_{cor}/t_{run})^{1/2}[1-C(t)]$, where t'_{cor} is a modified correlation time obtained by integration of $C^2(t)$ and t_{run} is the production period of the simulation [59]. Thus, the error of $C(t)$ is 0 at $t = 0$, but it tends to $(2t'_{cor}/t_{run})^{1/2}$ at long time. With t'_{cor} estimated for our model systems and the production periods of about 700 ps, the long-time errors for all considered correlation functions are lower than 0.02.

Fig. 4 presents the functions $C_{V_i}(t)$ calculated for various configurations of the D^+–$A1^-$–A2 system on the basis of MD simulations. In the framework of the linear response formalism these functions are equivalent to the response functions, which describe the solvation energy relaxation following the solute charge jump [64]. The common feature of all functions plotted in Fig. 4 is that nearly 60% of the total change in solvation energy is achieved within the first 100 fs. The next 100 fs is sufficient for more than 90% relaxation of the solvation energy. The average relaxation time $\langle \tau \rangle$, which can be estimated by integration of tacf, depends on the choice of the triad subunit as well as on the spatial arrangement of the triad. It is the longest for $A1^-$ unit (0.18 ps for the regular triangle to 0.21 ps for the linear triad) and changes from 0.15 to 0.18 ps in the case of D^+. It is worth noting that the above values of $\langle \tau \rangle$ agree quite reasonably with

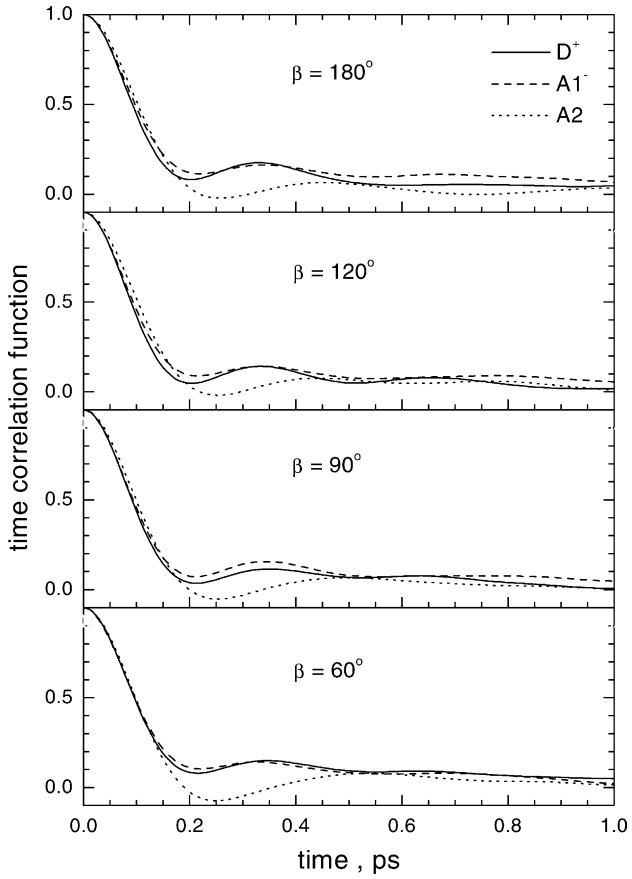

Fig. 4. Time auto-correlation functions of fluctuation in the electrical potential (Eq. (9)) produced by the acetonitrile molecules at the centers of each component of the triad calculated for different values of the angle β.

the longitudinal relaxation time τ_L which was estimated for liquid acetonitrile at 298 K as 0.2 ps [66]. The shortest $\langle\tau\rangle$ of the order of 0.12–0.14 ps is obtained for the atom A2 of the triad.

The above-mentioned values of $\langle\tau\rangle$ allow us to assume that the average solvation energy relaxation time for the whole triad of any shape should not exceed $\langle\tau\rangle_{max} = 0.21$ ps. In the present paper we describe the nonadiabatic ETs in the ionic triad using the equilibrium distribution in the free energy surfaces of the solvated D^+–$A1^-$–A2 systems. Such an approach is justified if the decay rate of the ionic triad, namely, the sum of rate constants for the backward (k_1) and forward (k_2) ETs is much smaller than $1/\langle\tau\rangle_{max} \approx 4.8\,ps^{-1}$. The ETs considered in the present work meet this condition. The time of the order of $\langle\tau\rangle_{max}$ is necessary also to complete the solvation of the D^+–$A1^-$–A2 triad, which arises from the respective neutral system by ET between the excited D and A1. Thus, for the rate constants k_1 and k_2 considerably slower than $4.8\,ps^{-1}$ we can neglect, in the first approximation, the effect of thermal equilibration of the ionic triad on the backward and forward ETs.

The decay of a fast component of the solvation response in the vicinity of a particular triad subunit can be estimated by fitting the early part of each tacf by the Gaussian function $\exp[-t^2/(2\tau_{sh}^2)]$ with a characteristic short-range correlation time τ_{sh}. The fittings performed over the time interval from 0 to 54 fs give τ_{sh} = 83–86 fs for the neutral subunit A2 and about 78 fs for the D^+ and $A1^-$. The fast part of the solvation response is governed by small amplitude inertial motions (mostly rotations) of solvent molecules in the close vicinity of the solute [64]. These motions should be slightly faster around the ionic components of the triad than around the neutral subunit and this is indeed reflected in the values of τ_{sh}. It seems that the aforementioned ordering of the average relaxation times $\langle\tau\rangle$, which is opposite for the ionic and neutral triad components to that of τ_{sh}, results from the slow, diffusive part of the solvation response. Most important contribution to this response comes from the reorganization of the first solvation shell of the triad. The shell is looser and less ordered around the A2 than around the D^+ and $A1^-$ (cf. Section 3.4) and this difference is the reason why the overall relaxation process is faster in the vicinity of the neutral moiety A2. Different behaviors of τ_{sh} and $\langle\tau\rangle$ for ionic and neutral subunits of the triad are reflected in the behaviors of τ_{sh} and $\langle\tau\rangle$ for the reaction coordinates q_1 and q_2 as shown below.

Fig. 5 presents the equilibrium time correlation functions (7) of fluctuations in the reaction coordinates associated with the backward and forward ETs and calculated for various spatial arrangements of the D^+–$A1^-$–A2 system on the basis of MD simulations. The oscillations in $C_1(t)$ are more clear and the overall relaxation process described by this function for all triad arrangements is slightly slower in comparison with $C_2(t)$. The average relaxation times $\langle\tau\rangle$ obtained by integration of (7) are 0.19–0.24 ps for the backward coordinate q_1, and 0.15–0.19 ps for the forward coordinate q_2. On the other hand, from the short-time Gaussian fittings to the tacfs for reaction coordinates we obtain τ_{sh} within the interval from 80 to 85 fs, but at each β the value for q_1 is slightly smaller than that for q_2. It is interesting to note that τ_{sh} for the two competitive ETs in the D^+–$A1^-$–A2 are shorter than τ_{sh} for the reaction coordinate associated with the ET between the excited donor D^* and the acceptor A1 in the neutral triads of various shape. The latter time was estimated in [32] as 92–98 fs.

To complete the study on the dynamical properties of the reaction coordinates, we construct the time cross-correlation functions (tccfs) of the form

$$C^{cross}_{V_2-V_i}(t) = \frac{\langle\delta V_2(0)\delta V_i(t)\rangle_I}{\rho_{2i}\sigma_{V_2}\sigma_{V_i}} \tag{8}$$

and

$$C^{cross}(t) = \frac{\langle\delta q_2(0)\delta q_1(t)\rangle_I}{\rho\sigma_1\sigma_2} \tag{9}$$

which describe the decay of the correlation between a particular pair of random quantities. In Eq. (8) V_i corresponds to the electrical potential at D^+ or A2, and ρ_{21} and ρ_{23} are the ensemble-averaged values of the correlation coefficients

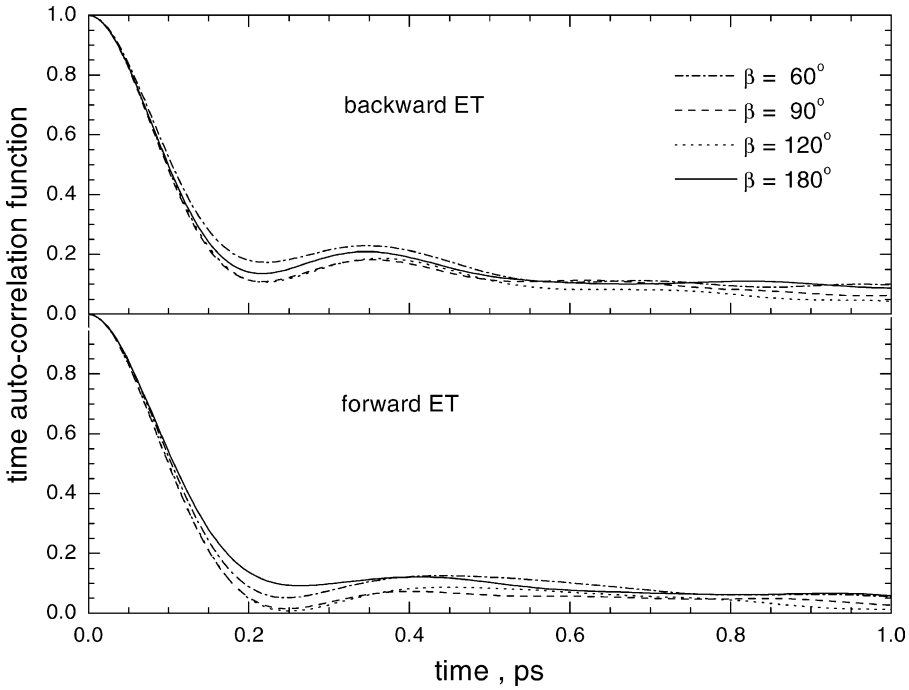

Fig. 5. Time auto-correlation functions (Eq. (10)) of fluctuations in the potential energy difference between $A1^-$ and D^+ (upper part) and between $A1^-$ and A2 (lower part) calculated for various triad shapes.

for the electrical potentials at the centers of $A1^-$ and D^+ or $A1^-$ and A2, respectively. For each spatial arrangement of the triad ρ_{21} is slightly lower (by about 0.02) than ρ_{23} and is decreasing from 0.40 for the regular triangle to 0.37 for the linear system.

Fig. 6 shows tccfs (8) obtained for various shapes of the triad. In all cases considered the correlation between V_1 and V_2 (full curves) decays faster than that between V_2 and V_3 (broken curves). It is especially pronounced for the *bent* triads with $\beta = 90^\circ$ and 120° and reflected in the early decay time constant τ_{sh}, which equals about 70 fs for $C^{cross}_{V_1-V_2}(t)$ and about 80 fs in the case of $C^{cross}_{V_2-V_3}(t)$. Different short-time behaviors of the two tccfs can be explained by the aforementioned ordering role of the electrostatic interactions between D^+ or $A1^-$ and the acetonitrile molecules in the close vicinity of the ionic part of the triad (cf. explanation to Fig. 4). The functions $C^{cross}_{V_1-V_2}(t)$ for $\beta > 60^\circ$ decay considerably faster than the corresponding functions $C^{cross}_{V_2-V_3}(t)$ also in the longer time scale.

It is worthwhile to note that tacfs (7) for the backward and forward ETs are related to tacfs (6) and tccfs (8) via theoretical relations of the form

$$C_1(t) = \frac{1}{\sigma_1^2}(\sigma_{V_1}^2 C_{V_1}(t) + \sigma_{V_2}^2 C_{V_2}(t) - 2\rho_{21}\sigma_{V_1}^2\sigma_{V_2}^2 C^{cross}_{V_2-V_1}(t)) \quad (10)$$

$$C_2(t) = \frac{1}{\sigma_2^2}(\sigma_{V_2}^2 C_{V_2}(t) + \sigma_{V_3}^2 C_{V_3}(t) - 2\rho_{23}\sigma_{V_2}^2\sigma_{V_3}^2 C^{cross}_{V_2-V_3}(t)) \quad (11)$$

These relations are fulfilled by the time correlation functions, correlation coefficients and variances obtained from our MD simulations for all triad shapes considered.

Fig. 7 presents the tccfs (9) of the reaction coordinates q_1 and q_2, calculated for various spatial arrangements of the triad subunits. The time constant τ_{sh} for the decay of the fast Gaussian component of $C^{cross}(t)$ increases from about 75 fs for the *bent* triads to 91 fs for the regular triangle and 105 fs for the linear D^+–$A1^-$–A2 system.

3.3. ET rates

By using the results in Figs. 1–3, we can construct the 2D Gaussian distribution (2) of the reaction coordinates q_1 and q_2. The free energy function $F(q_1, q_2)$ for the D^+–$A1^-$–A2 triad (redox State I) can be defined as

$$F(q_1, q_2) = -k_B T \ln \varphi(q_1, q_2) \quad (12)$$

and, like the distribution φ (Eq. (2)), it depends on the spatial arrangements of the triad subunits. Fig. 8 presents the contour maps of $F(q_1, q_2)$ which were obtained for the considered values of β.

The ETs between the redox States I → 0 and I → II occur along the intersections Γ of the relevant free energy surfaces in the 2D reaction coordinate space. With our choice of q_1 and q_2, $\Gamma_{I\to 0}$ and $\Gamma_{I\to II}$ are the straight lines parallel to one of the coordinate axes [29]. In other words, the intersection line $\Gamma_{I\to 0}$ for the backward ET is expressed by

$$q_1 = q_1^{\#}, \quad q_2 \in (-\infty, \infty) \quad (13)$$

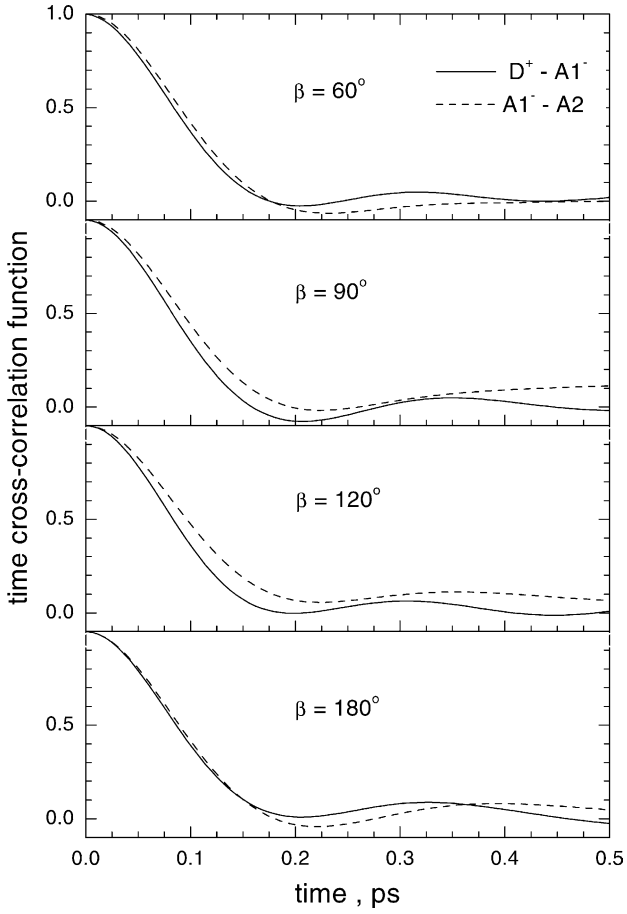

Fig. 6. Time cross-correlation functions (Eq. (11)) for the electrical potentials produced by the acetonitrile molecules on the D^+ and $A1^-$ (full line) and on the $A1^-$ and A2 (broken line) calculated for various values of the angle β.

whereas relations

$$q_1 \in (-\infty, \infty), \quad q_2 = q_2^{\#} \tag{14}$$

describe $\Gamma_{I\to II}$ associated with the forward ET. These intersection lines are shown schematically in Fig. 8. The values of $q_1^{\#}$ and $q_2^{\#}$ depend on the triad configuration and for each value of β are given by [29]

$$q_1^{\#}(\beta) = \lambda_1(\beta) - \Delta G_1 \tag{15}$$

$$q_2^{\#}(\beta) = -\lambda_2(\beta) + 2\lambda_{12}(\beta) - \Delta G_2 \tag{16}$$

where ΔG_1 and ΔG_2 are the free energy changes, λ_1 and λ_2 are the reorganization energies (Eq. (5)) and $\lambda_{12}(\beta) = \sigma_{12}^2(\beta)/2k_BT$.

The reaction rate constant k for a given transition is proportional to the probability of finding the system along the respective intersection line Γ

$$k \propto \iint_{\Gamma} \varphi(q_1, q_2)\, dq_1\, dq_2 \tag{17}$$

Since the joint probability density function $\varphi(q_1, q_2)$ is a 2D Gaussian, the integral in Eq. (17), with Γ defined by Eqs. (13) and (14), reduces to the value $\varphi_i(q_i^{\#})$ at $q_i = q_i^{\#}$ of the 1D normal distribution of the reaction coordinate q_i. In our approach the two ETs, at $q_1 = q_1^{\#}$ and $q_2 = q_2^{\#}$, do not interfere with each other because their rates are slower than the rate of the fluctuation of acetonitrile in the vicinity of the ionic triad. Thus, we could assume that the equilibrium free energy surface $F(q_1, q_2)$ is maintained and characterize each of the two ETs independently, using the respective 1D free energy curves [29–32].

The rate constants of charge recombination, $k_{I\to 0} \equiv k_1$, and charge shift, $k_{I\to II} \equiv k_2$, in the triad system with a given

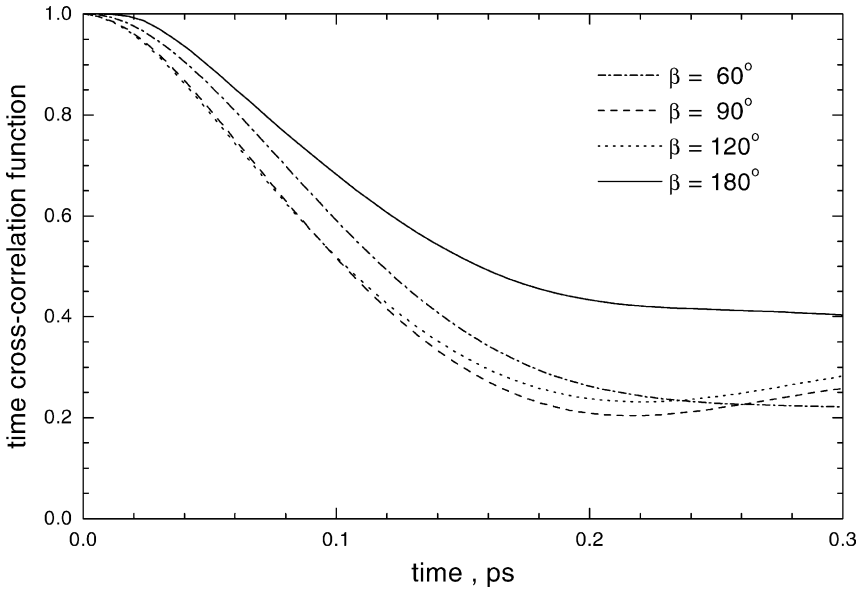

Fig. 7. Time cross-correlation functions (Eq. (12)) of fluctuations in the reaction coordinates q_1 and q_2 calculated for various triad shapes.

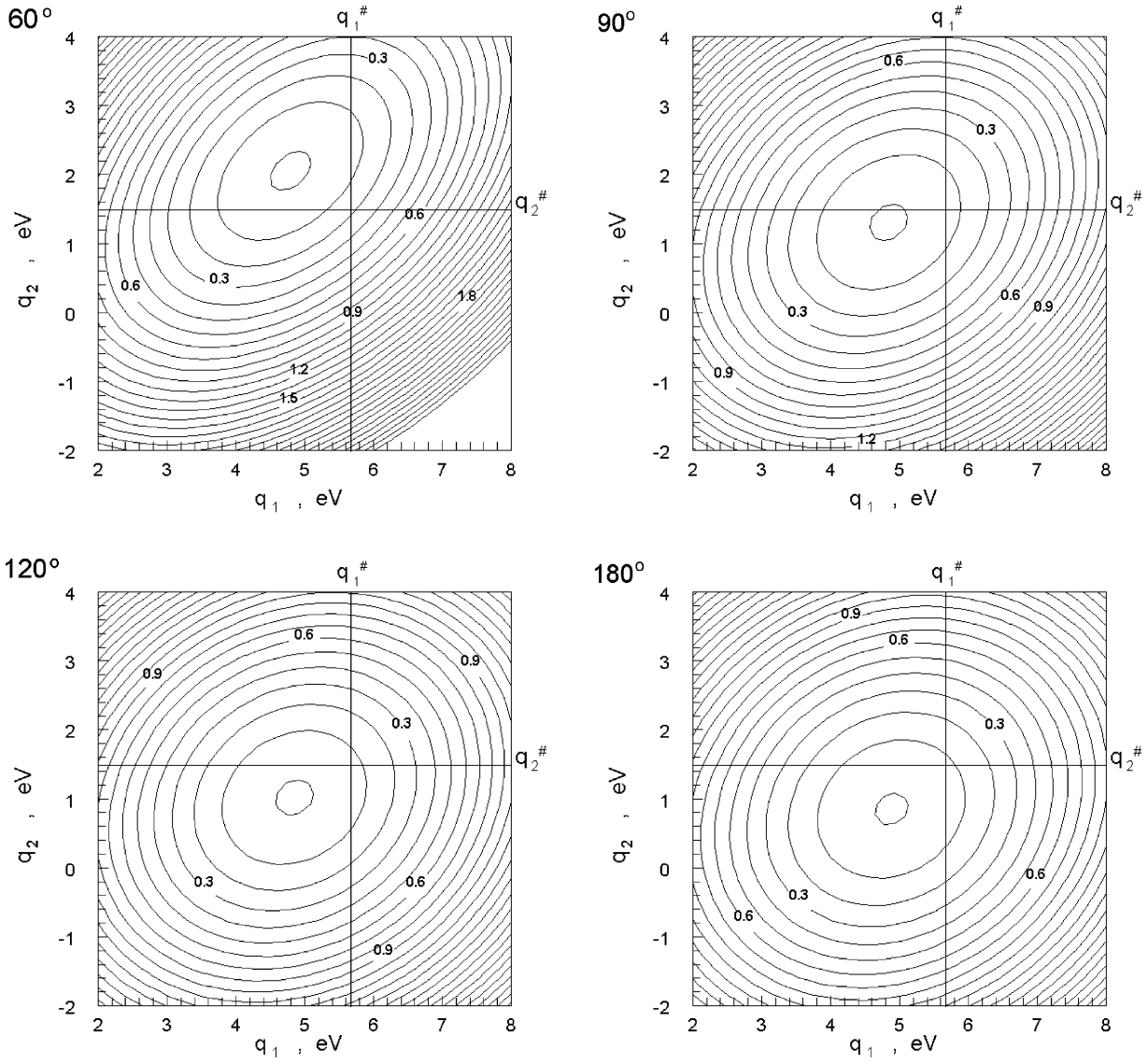

Fig. 8. Contour maps of the potential energy function for the D^+–$A1^-$–A2 supramolecule with various arrangements β of the subunits. The backward ET occurs along the line $q_1 = q_1^{\#}$, and the forward ET along $q_2 = q_2^{\#}$. The labels stand for the values of energy in units of eV, and the difference between successive contours is 0.1 eV.

spatial arrangement of the subunits are given by

$$k_1(\beta) = \frac{2\pi}{\hbar} J_1^2 \varphi_1[q_1^{\#}(\beta)] \tag{18}$$

and

$$k_2(\beta) = \frac{2\pi}{\hbar} J_2^2 \varphi_2[q_2^{\#}(\beta)] \tag{19}$$

respectively. In Eqs. (18) and (19) J_i for $i = 1, 2$ stands for the transfer integral

$$J_i = J_0 \exp[-\tfrac{1}{2}\alpha(R - 2r_a)] \tag{20}$$

with $R = 5.5$ Å, $r_a = 2.75$ Å and we take the constant parameters as $\alpha = 1.0\,\text{Å}^{-1}$ and $J_0 = 100\,\text{cm}^{-1}$. The same values of R, r_a, α, and J_0 were employed in our previous calculations of the charge separation rate constants in the neutral D–A1–A2 system [32]. As it was mentioned in Section 1, our main purpose is to describe the influence of solvent *molecularity* on ET processes in simple triad systems. From this point of view it seems reasonable to keep the same values of the parameters, which are connected mostly with the solute properties in order to minimize the number of variables introduced into the model.

In the present MD calculations $q_1^{\#}$ and the reorganization energy λ_1 depend slightly on the triad shape and, consequently, the rate constant k_1 changes with β. The variation of k_1 is, however, not very large. The value of $q_2^{\#}$ for the forward ET depends strongly on β (mostly via $\lambda_{12}(\beta)$), but this dependence is canceled to a large extent by the β-shift of the maximum of $\varphi_2[q_2(\beta)]$ distribution (cf. Fig. 2). The functions $k_1(\beta)$ and $k_2(\beta)$ calculated for constant energies

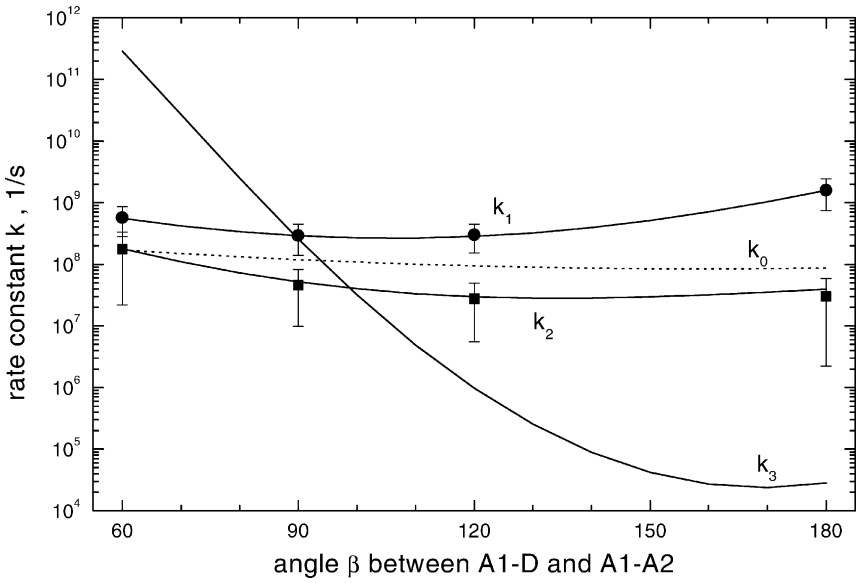

Fig. 9. β-dependence of the ET rate constants for charge recombination, k_1 (black circles with error bars), and charge shift, k_2 (black squares with error bars), in the ionic D^+–$A1^-$–A2 system as well as for the charge separation reactions k_0: D–A1–A2 → D^+–$A1^-$–A2 and k_3: D–A1–A2 → D^+–A1–$A2^-$ in the neutral triad obtained for the molecular model of the solvent. Calculations were performed for acetonitrile solutions at 291 K with $\Delta G_1 = \Delta G_2 = \Delta G_0 = -0.8$ eV and $\Delta G_3 = -1.6$ eV. The curves $k_0(\beta)$ and $k_3(\beta)$ are taken from [32].

$\Delta G_1 = \Delta G_2 = -0.8$ eV are presented in Fig. 9. The symbols with error bars in the figure show the rate constants k_1 and k_2 for the triad configurations, for which we performed the MD simulations. The full lines are obtained by utilizing in Eqs. (15)–(19) the second-order polynomial fittings to the MD values of $m_i(\beta)$, $\lambda_i(\beta)$ and $\lambda_{12}(\beta)$ performed for the whole β-interval. The errors in rate constants are evaluated from the errors of the respective MD values of means, reorganization energies, and also (in the case of k_2) the covariances $\sigma_{12}^2(\beta) = 2k_BT\lambda_{12}(\beta)$. The errors of $\sigma_{12}^2(\beta)$ were calculated from the time cross-correlation functions [59] and their values for the considered triad arrangements are between 4×10^{-4} and 6×10^{-4} eV^2.

In the figure we show also the rate constant $k_0(\beta)$ of the charge separation reaction D–A1–A2 → D^+–$A1^-$–A2 calculated for the free energy change $\Delta G_0 = -0.8$ eV [32]. As can be seen the functions $k_1(\beta)$, $k_2(\beta)$ and $k_0(\beta)$ differ appreciably from each other. To complete the comparison we plot additionally the rate constants $k_3(\beta)$ of the charge separation reaction: D–A1–A2 → D^+–A1–$A2^-$ obtained from MD results for $\Delta G_3 = -1.6$ eV [32]. With our choice of ΔG_i the MD value of k_3 for the linear system is rather small, whereas the successive steps: D–A1–A2 → D^+–$A1^-$–A2 → D^+–A1–$A2^-$ occur with rates 86.8 and 39.4 μs^{-1}, respectively. On the other hand, the back ET that reforms the neutral system D–A1–A2 is about 18 times faster than the forward reaction.

Relation between the calculated rate constants k_1 and k_2 inverts if we assume more negative values of the free energy change. It is illustrated in Fig. 10, which presents the energy gap law for these two processes in the case of the linear arrangement of the triad subunits. In the inverted region of both reactions, i.e., for ΔG beneath -2.4 eV, the charge shift occurs up to one order of magnitude faster than the charge recombination.

To characterize the relation between the rates of the competitive ETs in the ionic supramolecule D^+–$A1^-$–A2 we define the β-dependent quantity K_2

$$K_2(\beta) = \frac{k_2(\beta)}{k_1(\beta) + k_2(\beta)} \tag{21}$$

which we call the yield of the forward ET. For the purpose of the following comparison we assume equal values of the transfer integrals $J_1 = J_2$ in Eq. (21). The yield K_2 is presented in Fig. 11 as a function of $q_2^\#$ for different arrangements of the triad subunits. All curves are plotted for the constant difference $|q_1^\#(\beta) - q_1^{\min}(\beta)|$ equal to 0.8 eV, where $q_1^{\min}(\beta) \equiv m_1(\beta)$ denotes the value of $q_1(\beta)$ at the minimum of the free energy surface $F(q_1, q_2)$ constructed for the ionic system D^+–$A1^-$–A2 with a given geometry (see Fig. 8). The function $K_2(q_2^\#)$ has a flat maximum, which shifts by about 1.3 eV towards lower values of energy when β increases from 60° to 180°. The maximum values of the yield K_2 exceed 0.9 for all triad arrangements considered.

The shape and height of the function $K_2(q_2^\#)$ depend, however, on the assumed value of $q_1^\#$. Fig. 12 shows the functions obtained from MD calculations for the regular triangle and linear D^+–$A1^-$–A2 triads and for various values of $|q_1^\#(\beta) - q_1^{\min}(\beta)| = \delta_1$. As can be expected, the smallest K_2 are obtained in both cases for $\delta_1 = 0$, i.e., when the rate constant k_1 achieves its maximum value.

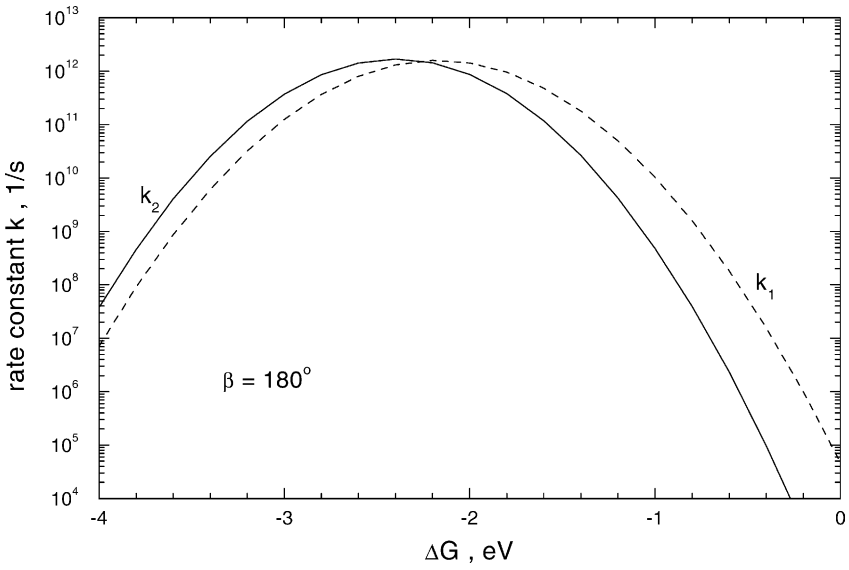

Fig. 10. Energy gap law for the backward ET (k_1) and the forward ET (k_2). The linear triad system D^+–A1$^-$–A2 in acetonitrile solvent at 291 K.

In the design of molecular devices for storing solar energy it is important to reach a relatively high value of K_2 and to accumulate a large amount of energy $\Delta E_{stor} = \Delta G_2 - \Delta G_1$ in a *final* charge-separated state. Hence, it can be interesting to analyze results of the present model from the energy-storage point of view for the D^+–A1–A2$^-$ triad as a *final* state. Fig. 13 shows the contour map of the product $K_2 \Delta E_{stor}$ as a function of the free energy changes ΔG_1 and ΔG_2 of the backward and forward ETs in the D^+–A1$^-$–A2 supramolecule with geometry described by the angle $\beta = 180^\circ$. As can be seen, the product $K_2 \Delta E_{stor}$ increases with the decrease of both ΔG_1 and ΔG_2 and is close to 1 for ΔG_1 lower than -3 eV. Such low values of ΔG_1 correspond to the inverted Marcus region of the charge recombination reaction (cf. Fig. 10) with $\delta_1 = q_1^{\#} - q_1^{min}$ larger than 0.8 eV (see Fig. 12). Let us take a fixed value of ΔG_1, say -3 eV. In this case the rate constant of the backward ET is also fixed at $k_1 = 0.12\,ps^{-1}$ and the yield K_2 is maximized when the rate constant k_2 of the forward reaction is maximized. The largest value of k_2 is obtained when $-\Delta G_2$ becomes equal to the reorganization energy λ_2, i.e., equal to 2.39 eV in the case of the linear triad system. For more negative values of ΔG_2 the value of K_2 and that of $\Delta G_2 - \Delta G_1$ both decrease, so the product $K_2 \Delta E_{stor}$ also decreases. On the other hand,

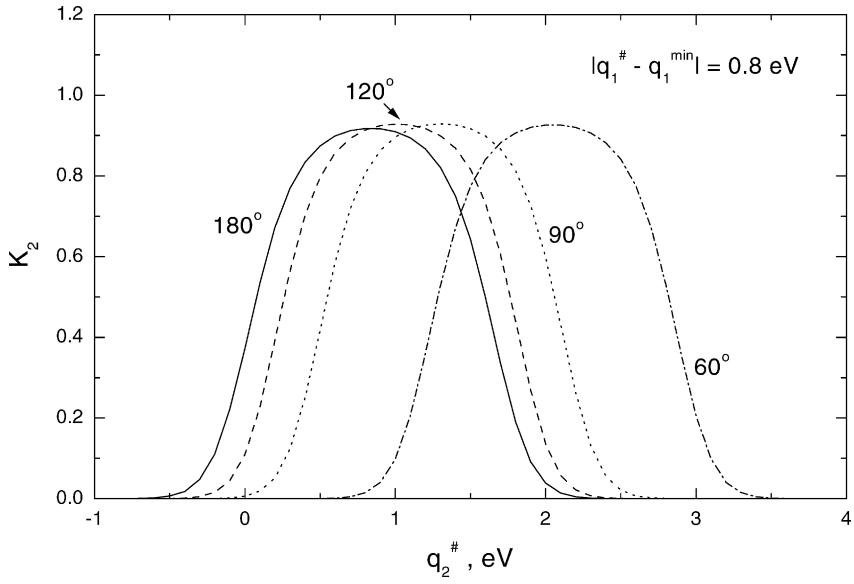

Fig. 11. Yield of the forward ET, K_2, as a function of $q_2^{\#}$ for different arrangements ($\beta = 60$, 90, 120, and 180°) of the D^+–A1$^-$–A2. q_1^{min} is the value of q_1 at the minimum of the respective free energy surface $F(q_1, q_2)$. Functions $K_2(q_2^{\#})$ are calculated for a constant difference of 0.8 eV between $q_1^{\#}(\beta)$ and $q_1^{min}(\beta)$. Acetonitrile solutions, 291 K.

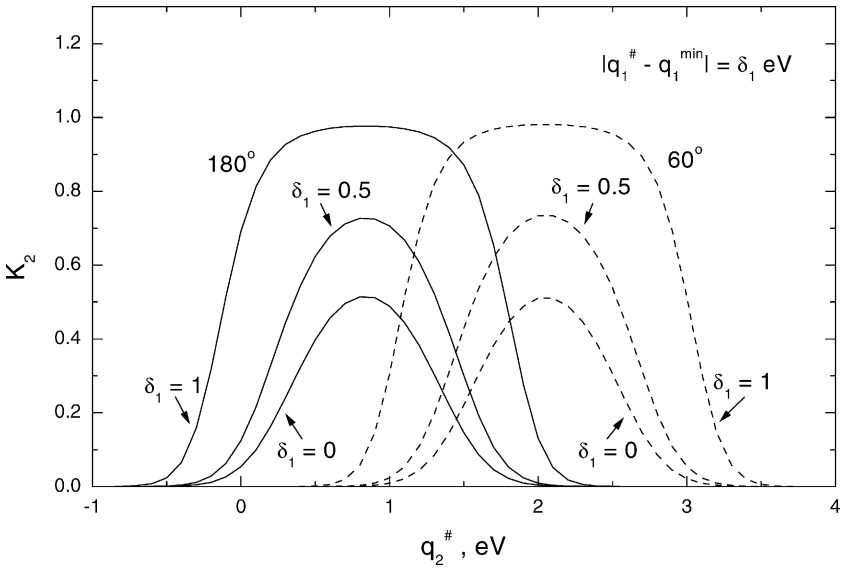

Fig. 12. Yield K_2 of the forward ET as a function of $q_2^{\#}$ for the D^+–$A1^-$–A2 triad with the linear ($\beta = 180°$) and the regular triangle ($\beta = 60°$) geometry. $q_1^{\#}(\beta)$ is shifted from $q_1^{min}(\beta)$ by $\delta_1 = 0$, 0.5, and 1 eV, respectively.

if we increase ΔG_2 the value of K_2 decreases, but the value of $\Delta G_2 - \Delta G_1$ increases and, consequently, $K_2 \Delta E_{stor}$ may increase in some case. It follows from this argument that the value of ΔG_2^{max}, which maximizes $K_2 \Delta E_{stor}$ should be slightly larger than $-\lambda_2$. In the considered case we have $\Delta G_2^{max} = -1.88$ eV and the optimized values of the rate constant k_2, the yield K_2, the energy ΔE_{stor}, and the product $K_2 \Delta E_{stor}$ are 0.5 ps^{-1}, 0.81, 1.12 and 0.91 eV, respectively. Similar relation between ΔG_2^{max} and λ_2 is held also for triads with other arrangements of the subunits and the optimized values of K_2, ΔE_{stor}, and the product $K_2 \Delta E_{stor}$ as functions of the angle β characterizing the geometry of the triad, are plotted in Fig. 14. The smallest value of $K_2 \Delta E_{stor}$, which has been obtained for $\beta = 120°$, is lower by less than 18% in relation to its largest value predicted for the regular triangle triad. The optimized yield K_2 does not depend practically on the triad geometry and the forward reaction for all considered systems is 3–4 times faster than the backward process.

The value of $-\Delta G_2$ obtained from our optimization is larger than that estimated for the natural RC and for the majority of artificial molecular devices of the form D–A1–A2 synthesized in order to capture solar energy. However, there

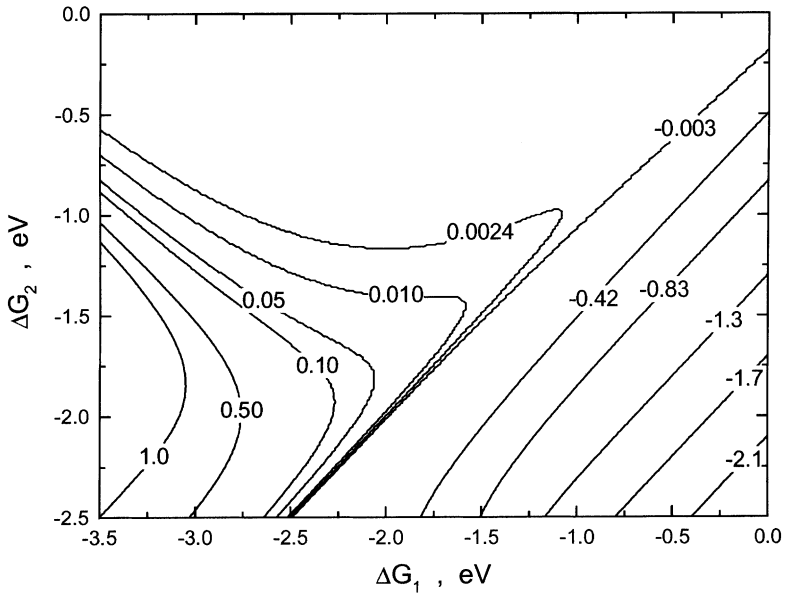

Fig. 13. Contour map of the quantity $K_2 \Delta G_{stor}$, where $\Delta G_{stor} = \Delta G_2 - \Delta G_1$, as a function of the free energy changes ΔG_1 and ΔG_2 of the forward and backward ETs for the linear D^+–$A1^-$–A2 supramolecule.

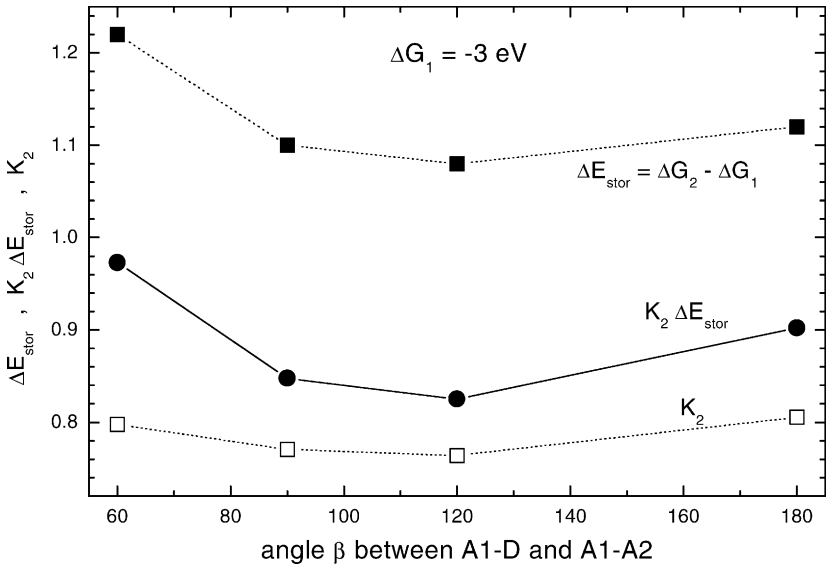

Fig. 14. Dependence of the yield K_2 of the forward ET, the energy $\Delta G_{stor} = \Delta G_2 - \Delta G_1$ accumulated in the D^+–A1–$A2^-$ state, and the product of these two quantities $K_2\Delta G_{stor}$ on the geometry of the D^+–$A1^-$–A2 triad. The free energy change of the charge recombination reaction is assumed to have a constant value $\Delta G_1 = -3$ eV.

are systems for which at least the free energy change ΔG_1 of the charge recombination reaction in D^+–$A1^-$–A2 is not very different from our optimized value and the reaction itself occurs in the inverted Marcus region. For instance, Lawson et al. [25] considered the series of compounds, in which three chromophores: DMA (*N*,*N*-dimethylaniline), DMN (dimetoxynaphthalene), and DCV (dicyanovinyl), are connected via bridges comprising several linearly fused norbornyl and bicyclo[2.2.0]hexyl units [25]. The Gibbs free energies $-\Delta G_1$ and $-\Delta G_2$ estimated for this triad in acetonitrile are of the order of 3.5 and ∼1 eV, respectively. In benzene solution the value of $\Delta G_2 - \Delta G_1$ is even higher and equals 3.4 eV. Thus, the efficiency of energy storage in their system is better than in our optimization. Another example is a UV-absorbing molecular triad based on aromatic imide chromophores, for which $-\Delta G_1$ and $-\Delta G_2$ in toluene solution are equal to about 2.7 and 0.9 eV, respectively [26]. The authors estimated also the rate constant of the forward ET for their triad as 2.3 ns^{-1}. Imahori et al. [27] synthesized a porphyrin–pyromellitimide–C_{60} triad with energy levels of the D^*–A1–A2, D^+–$A1^-$–A2, and D^+–A1–$A2^-$ states equal to 2.06, 1.92 and 1.84 eV, respectively, and nearly equal rate constants for the forward and backward ETs (16 and 17 ns^{-1}) in dioxane solution. Similarly, for the triad ANI–NI–PI studied by Lukas at al. [67], where ANI is a 4-(*N*-piperidinyl)-1,8-naphthaleneimide electron donor, and NI and PI are 1,8:4,5-naphthalenediimide and pyromellitimide acceptors, respectively, the ANI^+–PI–NI^- state in toluene solution lies approximately 0.08 eV below that of ANI^+–PI^-–NI. Additionally, the rate constant of the forward ET in ANI^+–PI^-–NI is more than two orders of magnitude larger than that for the backward reaction. Thus, according to our optimization criterion, this triad would be an example of very efficient system for storing solar energy. In the triad designed by Osuka et al. [24] and composed of fixed-distance porphyrin–oxochlorin–pyromellitdimide, the D^*–A1–A2, D^+–$A1^-$–A2, and D^+–A1–$A2^-$ states in DMF have energies 1.91, 1.75 and 1.46 eV, respectively. They found that the polar solvent although enables the sequential ETs: D^*–A1–A2 → D^+–$A1^-$–A2 → D^+–A1–$A2^-$, it enhances rate of the energy wasteful charge recombination process in D^+–$A1^-$–A2, decreasing the quantum yield of the final, long-lived D^+–A1–$A2^-$ state.

The aforementioned examples show that the value of $K_2\Delta E_{stor}$ in solvents of high polarity is lower than that in nonpolar solvents. Especially, the energy $\Delta E_{stor} = \Delta G_2 - \Delta G_1$ considerably decreases with the increase of polarity of the environment. To maximize the product $K_2\Delta E_{stor}$ the free energy change of the forward reaction ΔG_2 should have a small negative value. As we pointed in the previous paragraph the solvent reorganization energy λ_2 connected with this reaction should be smaller than $-\Delta G_2$ and this condition can be fulfilled rather by solvents of low polarity.

3.4. Solvent structure around the triad system

The time correlation functions in Figs. 4–7 show clearly differences in dynamics of the random variables eV_i and $e(V_i - V_j)$ constructed for the electrostatic potentials on different subunits of the D^+–$A1^-$–A2 system with various geometry described by the angle β. These differences can be connected with the average arrangement of solvent molecules around the triad, which is characterized for a given β by a set of solute–solvent radial distribution functions (RDFs). Using molecular configurations generated in

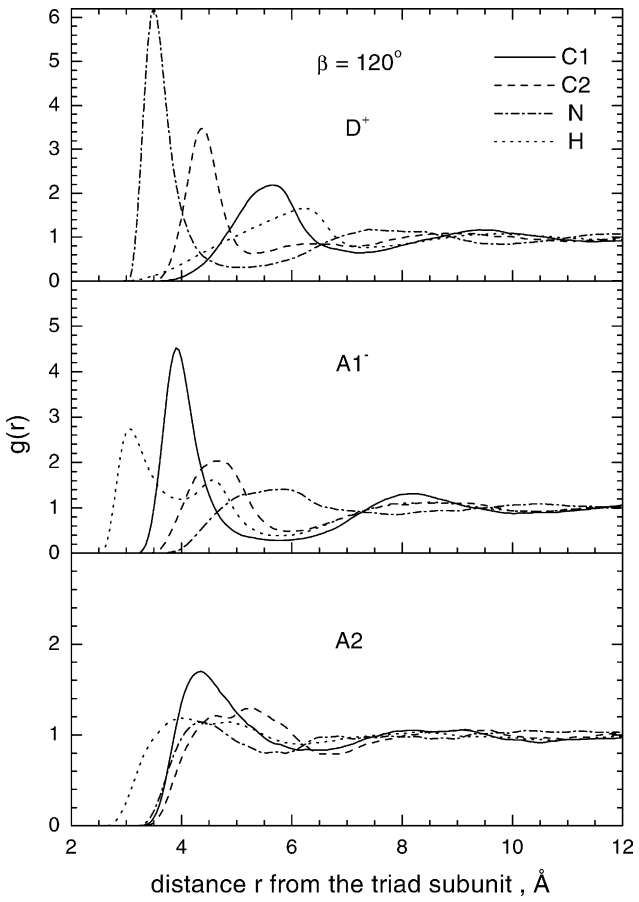

Fig. 15. RDFs describing the radial distributions of the particular sites of the acetonitrile molecules from D^+ (upper part), $A1^-$ (middle part), and A2 (lower part) subunits of the triad with $\beta = 120^\circ$. C_1 and C_2 stand for carbon sites of the methyl and cyanide groups, respectively.

equilibrium simulation runs, we calculated four sets of the RDFs for distances between each subunit of the triad and each site (atom) of the acetonitrile molecules.

Fig. 15 shows these RDFs obtained for the triad with angle $\beta = 120^\circ$. The functions in the figure can be directly compared with the atom-site RDFs of [32] for the neutral triad D–A1–A2. As expected, the presence of charge on D^+ and $A1^-$ results in a very strong correlation of acetonitrile molecule positions in the vicinity of the triad. The strongest correlation occurs for the N sites around D^+ ion. The first peak height of the D^+–N RDF equals 6.21 as compared to 1.12 for that of the D–N function in [32]. The former peak is also considerably higher than the first maximum of the D^+–C_2 $g(r)$ that is shifted from the former peak by 0.85 Å towards larger r. The integrated coordination numbers up to the first minimum of these two RDFs are $n_N = 7.8$ and $n_{C_2} = 8.0$, respectively. Since the C_2 site is close to the center of mass of CH_3CN, we can say that the latter minimum at $r = 5.3$ Å defines the first solvation layer of D^+. Thus, eight acetonitrile molecules forming this layer have their nitrogens directed toward the cation. From the positions of the main peaks of the N and C_2 RDFs we can infer that the average orientation of these solvent molecules is characterized by the angle $\angle(D^+–N–C_2) \approx 130^\circ$. The spatial extent of the first solvation shell of D^+ is shorter by 1.35 Å than that of the D atom in the neutral triad.

The closest to the $A1^-$ moiety of the triad are hydrogens of acetonitrile molecules. We obtained identical RDFs for each proton of the CH_3 group. The $A1^-$–H $g(r)$ has two distinct maxima, one at 3.05 Å and the other at 4.55 Å. It indicates that rotation of the methyl group is considerably limited in the vicinity of the anion. The minimum between the two hydrogen peaks is at 3.95 Å and it corresponds to the position of the first maximum in the $A1^-$–C_1 RDF. This maximum together with the first peak of the $A1^-$–C_2 RDF shows that acetonitrile molecules in the vicinity of the anion prefer orientations for which the average angle $\angle(A1^-–C_1–C_2) = 109.7^\circ$. The integration of the $A1^-$–C_1 $g(r)$ up to 3.95 Å gives $n_{C_1} = 3.33$ and the first maximum of the hydrogen RDFs corresponds to 2.78 atoms. These data and a detailed analysis of the H, C_1 and C_2 RDFs suggest that one of the methyl protons can be directed towards the $A1^-$ with the average angle $\angle(A1^-–C_1–H) \approx 30^\circ$. The distribution of positions of the other two protons is described by the second maximum of the $A1^-$–H functions. The first minimum of the anion-C_1 RDF is at 5.75 Å and the integrated coordination number up to this point is $n_{C_1} = 9.18$. The first coordination shell of $A1^-$ as composed of nine acetonitrile molecules was confirmed also by integration of C_2 and H RDFs. The spatial extend of this shell is equal to 5.95 Å.

The A2-site RDFs are similar to the distribution functions presented in [32] for the side atoms of the neutral triad. Correlation of the methyl group positions around A2 is, however, slightly stronger for the D^+–$A1^-$–A2 system. For example, the ratio of the peak heights of the C_1 RDFs for the two triads is equal to 1.36. The minimum of the A2–C_2 RDF is at 6.75 Å and we can expect 12 or 13 solvent molecules in the first solvation layer of the atom A2.

The concentration of C_2 sites in the first solvation shell of the cation equals $c_s(D^+) = 0.017\,Å^{-3}$ and we can assume that this value corresponds to the concentration of solvent molecules around D^+. Note that $c_s(D^+)$ is substantially higher as compared to the corresponding values for both the bulk acetonitrile ($0.012\,Å^{-3}$) and the vicinity of the D atom in the neutral triad ($0.010\,Å^{-3}$). The average concentration of the C_2 sites in the neighborhood of the ion $A1^-$ is $c_s(A1^-) = 0.013\,Å^{-3}$. However, the concentration of protons in the close vicinity of the anion is much higher and equals $0.056\,Å^{-3}$. These data clearly show that the relaxation process around $A1^-$ should be affected by very strong steric effects, which slow down the rotation of acetonitrile molecules in this region. Thus, it is not surprising that the average relaxation time $\langle\tau\rangle$, estimated by integration of the time correlation function (6), is longer for $A1^-$ than for D^+. The shortest $\langle\tau\rangle$ obtained for A2 is consistent with the smallest solvent concentration $c_s(A2) = 0.011\,Å^{-3}$, which was estimated from the first peak of the A2–C_2 RDF.

The RDFs for other spatial arrangements of the triad are similar to the functions presented in Fig. 15. It is interesting to note, however, that all the RDFs for the linear triad start at distances r_{st}, which are much shorter as compared to r_{st} for other triad shapes. The integrated coordination numbers for these small distances are very low. The most pronounced variations with β are observed among the RDFs for A2 moiety. For instance, the intensity of the first peak of the A2–C_1 RDF is considerably lower for a regular triangle than for other arrangements of the triad. The integrated coordination number n_{C_1} to the first minimum of the C_1 function is 9.1 for $\beta = 60^\circ$ and rises to 10.4 in the case of the linear system. Correlation of proton positions around A2 is also the weakest for $\beta = 60^\circ$. The solvation shell of A2 in the regular triangle system has a radius of 6.55 Å and it contains 11 acetonitrile molecules. This shell expands to 6.80 Å and 13 acetonitriles as β reaches 180°.

Differences in the average solvent structure around triads can be expressed globally by the radial charge distributions shown in Fig. 16. We calculated the total charge $T(r)$ inside the sphere of radius r around each subunit of a triad by evaluating the integrated coordination numbers $n_k(r)$ at the distance r for all sites of the acetonitrile molecules and summing $n_k(r)$ multiplied by the respective partial charges Q_k. In the figure we plotted $T(r)$ as a function of the distance r from the subunit D^+, $A1^-$ and A2, respectively, for the triads of various geometry. As can be seen, the charge distributions around the ionic subunit D^+ as well as those around the $A1^-$ are quite similar for all β considered. The first peak of $T(r)$ for the neutral moiety A2 is also independent on the triad shape. However, contribution from partial charges on more distant acetonitrile molecules causes difference between distribution functions around A2 for various triads.

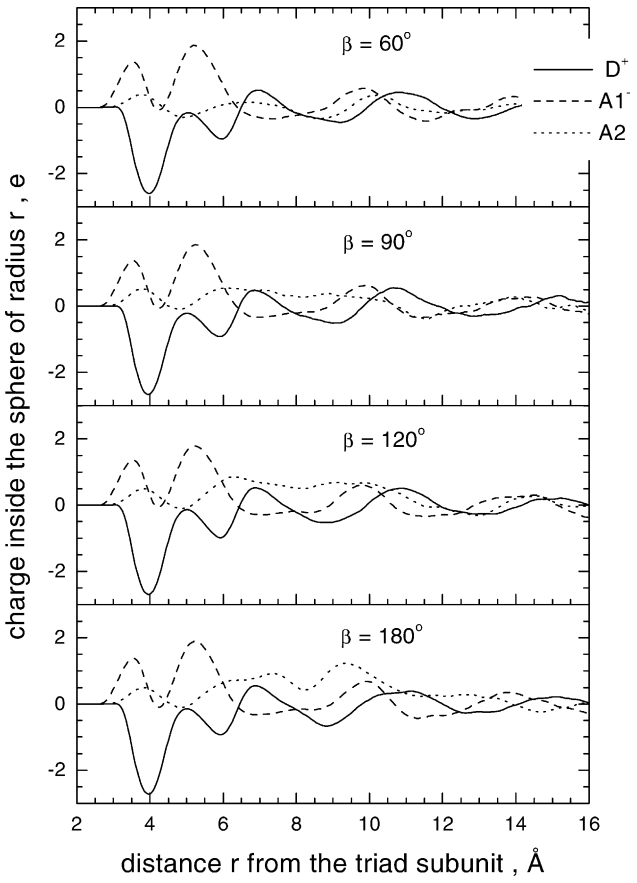

Fig. 16. Total charge of the sites of the acetonitrile molecules, which are enclosed within a sphere of radius r around the D^+ (full line), $A1^-$ (dashed line), and A2 (dotted line) subunits of the triads with $\beta = 60^\circ$, 90°, 120° and 180°, respectively, as a function of r.

4. Concluding remarks

We have considered competition between the nonadiabatic charge separation D^+–$A1^-$–A2 → D^+–A1–$A2^-$ and the charge recombination D^+–$A1^-$–A2 → D–A1–A2 in a model triad system D^+–$A1^-$–A2 immersed in acetonitrile solvent at room temperature. To treat these ETs, we have employed two reaction coordinates $q_1 = e(V_2 - V_1)$ and $q_2 = e(V_2 - V_3)$, and constructed the 2D free energy surface $F(q_1, q_2)$ for the triads of various geometry in acetonitrile solutions by MD computer simulations. Each of the two reactions occurs at the intersection of the free energy surfaces of the reactant and the respective product, and this intersection is a straight line parallel to one of the coordinate axes, q_1 or q_2. Positions of these lines can be changed by changing electronic properties of the triad moieties. In the nonadiabatic limit the ET rate constant is expressed in terms of the equilibrium distribution in the free energy surface.

The stochastic properties of the reaction coordinates as well as the triad geometry dependence of the ET rate constants obtained in our calculations differ considerably from predictions of the models, in which the solvent is treated as a dielectric continuum. Dynamical properties of the reaction coordinates for the ionic and neutral systems are closely correlated with the dynamics of the solvent surrounding the triads. The latter sometimes deviates significantly from our expectations based on the results for solvation of single neutral or ionic molecules.

Our calculations show the role of molecularity of the polar solvent in description of the competitive ET reactions between subunits of the triad system modeled in the simplest possible way. We hope that the present results can be a good basis for introducing further refinements and constructing more realistic theoretical models of the photoinduced ETs in supramolecular systems.

The reorganization energies estimated in our calculations for the ionic triads are comparable with the values of λ for the corresponding neutral triads. They are higher, however, than λ predicted on the basis of the continuum model of the solvent for majority of synthesized supramolecular systems. To verify and improve our estimation of λ it would be necessary to take into consideration the internal structure of a supramolecule that is usually composed of many atoms and

characterized by spatial distribution of partial charges [65]. The triad system constructed in our approach does not exemplify an efficient molecular device for capturing and storing solar energy. The amount of energy stored in the final charge-separated state is too low, and a reasonably high yield of the forward ET is obtained only under the assumption that both reactions are noticeably exoergonic. Our model, however, adopts a very approximate expression for the transfer integral and does not discriminate between the strengths of coupling of the reactant state with that of each of the products. Optimizing the values of the pre-exponential factors in the rate constant formulas for both reactions we can improve the relation between the backward and forward ET rates.

References

[1] D. Gust, T.A. Moore, Top. Curr. Chem. 159 (1991) 103.
[2] D. Gust, T.A. Moore, A.L. Moore, Pure Appl. Chem. 70 (1998) 2189; D. Gust, T.A. Moore, A.L. Moore, Acc. Chem. Res. 26 (1993) 198.
[3] M.R. Wasielewski, Chem. Rev. 92 (1992) 435.
[4] G.P. Wiederrecht, S. Watanabe, M.R. Wasielewski, Chem. Phys. 176 (1993) 601.
[5] J.R. Bolton, N. Mataga, G. McLendon (Eds.), Electron Transfer in Inorganic, Organic, and Biological Systems, American Chemical Society, Washington, 1991.
[6] F.S. Sterrett (Ed.), Alternative Fuels and the Environment, Lewis, Boca Raton, 1995.
[7] J.-P. Sauvage, J.-P. Collin, J.-C. Chambron, S. Guillerez, Ch. Coudret, V. Balzani, F. Barigelletti, L. De Cola, L. Flamingi, Chem. Rev. 94 (1994) 993.
[8] V. Balzani, Tetrahedron 48 (1992) 10443.
[9] V. Balzani, S. Campagna, G. Denti, S. Serroni, in: E. Kochanski (Ed.), Photoprocesses in Transition Metal Complexes, Biosystems and Other Molecules, Experiment and Theory, Kluwer Academic Publishers, Dordrecht, 1992, p. 233.
[10] G. Denti, S. Campagna, L. Sabatino, S. Serroni, M. Ciano, V. Balzani, in: E. Pelizzetti, M. Schiavello (Eds.), Photochemical Conversion and Storage of Solar Energy, Kluwer Academic Publishers, Dordrecht, 1991, p. 27.
[11] S.-C. Hung, A.N. Macpherson, S. Lin, P.A. Liddell, G.R. Seely, A.L. Moore, T.A. Moore, D. Gust, J. Am. Chem. Soc. 117 (1995) 1657.
[12] D. Gust, T.A. Moore, A.L. Moore, A.N. Macpherson, A. Lopez, J.M. DeGraziano, I. Gouni, E. Bittersmann, G.R. Seely, F. Gao, R.A. Nieman, X.C. Ma, L.J. Demanche, S.C. Hung, D.K. Luttrull, S.J. Lee, P.K. Kerrigan, J. Am. Chem. Soc. 115 (1993) 11141.
[13] P.A. Liddell, D. Kuciauskas, J.P. Sumida, B. Nash, D. Nguyen, A.L. Moore, T.A. Moore, D. Gust, J. Am. Chem. Soc. 119 (1997) 1400.
[14] D. Gosztola, M.P. Niemczyk, M.R. Wasielewski, J. Am. Chem. Soc. 120 (1998) 5118.
[15] D. Carbonera, M. Di Valentin, C. Corvaja, G. Agostini, G. Giacometti, P.A. Liddell, D. Kuciauskas, A.L. Moore, T.A. Moore, D. Gust, J. Am. Chem. Soc. 120 (1998) 4398.
[16] G.R. Fleming, R. van Grondelle, Phys. Today 47 (1994) 48.
[17] G. Steinberg-Yfrach, P.A. Liddell, S.-Ch. Hung, A.L. Moore, D. Gust, T.A. Moore, Nature 386 (1997) 239.
[18] G. Steinberg-Yfrach, J.-L. Rigaud, E.N. Durantini, A.L. Moore, D. Gust, T.A. Moore, Nature 392 (1998) 479.
[19] A. Harriman, F. Odobel, J.-P. Sauvage, J. Am. Chem. Soc. 116 (1994) 5481.
[20] R.J. Willemse, J.W. Verhoeven, A.M. Brouwer, J. Phys. Chem. 99 (1995) 5753.
[21] S.I. van Dijk, P.G. Wiering, C.P. Groen, A.M. Brouwer, J.W. Verhoeven, W. Schuddeboom, J.M. Warman, J. Chem. Soc., Faraday Trans. 91 (1995) 2107.
[22] A.M. Brouwer, C. Eijckelhoff, R.J. Willemse, J.W. Verhoeven, W. Schuddeboom, J.M. Warman, J. Am. Chem. Soc. 115 (1993) 2988.
[23] N. Sabbatini, M. Guardigli, J.M. Lehn, Coord. Chem. Rev. 123 (1993) 201.
[24] A. Osuka, S. Marumo, K. Maruyama, N. Mataga, Y. Tanaka, S. Taniguchi, T. Okada, I. Yamazaki, Y. Nishimura, Bull. Chem. Soc. Jpn. 68 (1995) 262;
A. Osuka, S. Nakajima, K. Maruyama, N. Mataga, T. Asahi, I. Yamazaki, Y. Nishimura, T. Ohno, K. Nozaki, J. Am. Chem. Soc. 115 (1993) 4577.
[25] J.M. Lawson, M.N. Paddon-Row, W. Schuddeboom, J.M. Warman, A.H.A. Clayton, K.P. Ghiggino, J. Phys. Chem. 97 (1993) 13099.
[26] K. Hasharoni, H. Levanon, S.R. Greenfield, D.J. Gosztola, W.A. Svec, M.R. Wasielewski, J. Am. Chem. Soc. 117 (1995) 8055;
K. Hasharoni, H. Levanon, S.R. Greenfield, D.J. Gosztola, W.A. Svec, M.R. Wasielewski, J. Am. Chem. Soc. 118 (1996) 10228.
[27] H. Imahori, K. Yamada, M. Hasegawa, S. Taniguchi, T. Okada, Y. Sakata, Angew. Chem. Int. Ed. Engl. 36 (1997) 2626.
[28] D.G. Johnson, M.P. Niemczyk, D.W. Minsek, G.P. Wiederrecht, W.A. Svec, G.L. Gaines, M.R. Wasielewski, J. Am. Chem. Soc. 115 (1993) 5692;
M.R. Wasielewski, G.L. Gaines, G.P. Wiederrecht, W.A. Svec, M.P. Niemczyk, J. Am. Chem. Soc. 115 (1993) 10442.
[29] J. Najbar, M. Tachiya, J. Phys. Chem. 98 (1994) 199.
[30] M. Fushiki, M. Tachiya, J. Phys. Chem. 98 (1994) 10762.
[31] T. Motylewski, J. Najbar, M. Tachiya, Chem. Phys. 212 (1996) 193.
[32] M. Hilczer, M. Tachiya, J. Phys. Chem. 100 (1996) 8815.
[33] A.V. Barzykin, M. Tachiya, Chem. Phys. Lett. 285 (1998) 150.
[34] M. Marchi, J.N. Gehlen, D. Chandler, M.D. Newton, J. Am. Chem. Soc. 115 (1993) 4178.
[35] W.W. Parson, Z.T. Chu, A. Warshal, Biochim. Biophys. Acta 251 (1990) 1017.
[36] A. Warshel, W.W. Parson, Annu. Rev. Phys. Chem. 42 (1991) 279.
[37] A. Warshel, Z.T. Chu, W.W. Parson, J. Photochem. Photobiol. A 82 (1994) 123.
[38] M. Fushiki, M. Tachiya, Chem. Phys. Lett. 255 (1996) 83.
[39] L.D. Zusman, D.N. Beratan, J. Chem. Phys. 110 (1999) 10468.
[40] A. Okada, T. Bandyopadhyay, M. Tachiya, J. Chem. Phys. 110 (1999) 3509;
A. Okada, T. Bandyopadhyay, J. Chem. Phys. 111 (1999) 1137.
[41] J. Najbar, M. Tachiya, J. Photochem. Photobiol. A 95 (1996) 51; K. Pirowska, J. Najbar, Acta Phys. Pol. A 94 (1998) 637.
[42] S.S. Skourtis, S. Mukamel, Chem. Phys. 197 (1995) 367.
[43] M.D. Newton, J. Electroanal. Chem. 438 (1997) 3.
[44] L.W. Ungar, M.D. Newton, G.A. Voth, J. Phys. Chem. B 103 (1999) 7367.
[45] M.D. Newton, Adv. Chem. Phys. 106 (1999) 303.
[46] N. Gayathri, B. Bagchi, J. Phys. Chem. A 103 (1999) 8496.
[47] M. Bixon, J. Jortner, M.E. Michel-Beyerle, Chem. Phys. 197 (1995) 389.
[48] M.A. Thompson, G.K. Schenter, J. Phys. Chem. 99 (1995) 6374.
[49] M. Bixon, J. Jortner, J. Phys. Chem. 90 (1986) 3795.
[50] K. Schulten, M. Tesch, Chem. Phys. 158 (1991) 421.
[51] S. Creighton, J.-K. Hwang, A. Warshel, W.W. Parson, J. Norris, Biochemistry 27 (1988) 774.
[52] W.W. Parson, Z.-T. Chu, A. Warshel, Biochim. Biophys. Acta 1017 (1990) 251.
[53] D. Chandler, J.N. Gehlen, M. Marchi, in: Y. Gauduel, P.J. Rossky (Eds.), Ultrafast Reaction Dynamics and Solvent Effects, Symposium Series, Institute of Physics, 1994, p. 50.
[54] R.A. Marcus, N. Sutin, Biochim. Biophys. Acta 811 (1985) 265.
[55] H.J. Böhm, I.R. McDonald, P.A. Madden, Mol. Phys. 49 (1983) 347.
[56] H.J. Böhm, R.M. Lynden-Bell, P.A. Madden, I.R. McDonald, Mol. Phys. 51 (1984) 761.
[57] T. Ohba, S. Ikawa, Mol. Phys. 73 (1991) 999.
[58] A.S. Al-Mubarak, G. Del Mistro, P.G. Lethbridge, N.Y. Abdul-Sattar, A.J. Stace, Faraday Discuss., Chem. Soc. 86 (1988) 209.

[59] M.P. Allen, D.J. Tildesley, Computer Simulation of Liquids, Clarendon, Oxford, 1987.
[60] W. Smith, D. Fincham, CCP5 Program Library, Science and Research Council, Daresbury Laboratory, Warrington, UK, 1982.
[61] D.J. Adams, G.S. Dubey, J. Comput. Phys. 72 (1987) 156.
[62] M. Tachiya, J. Phys. Chem. 97 (1993) 5911.
[63] H.A. Yu, M. Karplus, J. Chem. Phys. 89 (1988) 2366.
[64] M. Maroncelli, J. Chem. Phys. 94 (1991) 2084.
[65] M. Hilczer, M. Tachiya, Chem. Phys. Lett. 295 (1998) 337; M. Hilczer, M. Tachiya, J. Mol. Liq. 86 (2000) 97.
[66] J. Barthel, K. Bachhuber, R. Buchner, J.B. Gill, M. Kleebauer, Chem. Phys. Lett. 167 (1990) 63.
[67] A.S. Lukas, S.E. Miller, M.R. Wasielewski, J. Phys. Chem. B 104 (2000) 931.